Removal of U(VI) from aqueous solution using AO-artificial zeolite

Peng Liu[1] · Qiang Yu[1,2] · Xu Zhang[3] · Jiaqi Chen[1] · Yun Xue[1] · Fuqiu Ma[1]

Abstract

Amidoxime (AO) based adsorbents have been proposed as low cost and efficient adsorbent for U(VI). Herein, we present a simple strategy for preparing AO modified artificial zeolite. The composition and morphology of the materials have been confirmed via XRD, FT-IR, TGA and SEM. The AO-artificial zeolite was synthesised as an efficient adsorbent for adsorbing U(VI). The critical factors affecting U(VI) adsorption from aqueous solution were exploited, such as pH, contact time, temperature and adsorbent dosage. This study reveals AO-artificial zeolite, along with a low-cost, environmentally friendly and facile synthesis, can be regarded as a promising material for uranium-containing wastewater treatment.

Keywords U(VI) · Artificial zeolite · Adsorption · Amidoxime based adsorbent

Introduction

With the rapid development of human modernization, nuclear power is developed vigorously because of the low greenhouse gas emissions and high energy density [1]. Uranium is the most major fuel for the generation of electricity in the nuclear power industry [2]. However, uranium also has chemical and radioactive toxicity, on condition that a large quantity of uranium discharged into our environment, it would be accumulated in human beings through the food chain and lead to health problems [3, 4]. Therefore, numerous methods have been used to removal of U(VI) from aqueous solutions, such as extraction [5, 6], coprecipitation [7], flotation [8], membrane dialysis [9], adsorption [10, 11] and so on. Among these methods, adsorption has attracted much attention due to its easy operation and high efficiency.

Recently, various kinds of adsorbents, such as amine [12], carboxylates [13], carbon materials [14], polymers [15, 16], magnetic materials [17] and metal organic frame works [18], have been developed for the removal of U(VI) from aqueous solution. For most adsorbents, however, the defect of disperse in aqueous during adsorption process restrict their further industrial applications [19]. Thus, adsorbents suitable for commercialized need to be developed for uranium adsorption. Artificial zeolite has attracted considerable attention because of its regular mesoporous pore structure and chemical and physical stabilities. Nevertheless, only a few functional groups can provide the adsorption active sites for uranium. Among them, amidoxime (AO) group has acidic oxime and amino groups, and the presence of the functional groups shown great potential to form complexes with U(VI) [20, 21]. Thus, it is important to modify artificial zeolite with AO group for U(VI) adsorption.

Hence, the AO functionalized artificial zeolite are prepared. The X-ray diffraction (XRD), fourier transform infrared spectra (FT-IR), scanning electron microscopy (SEM), N_2 adsorption–desorption, and thermogravimetric analysis (TGA) are used to characterize the properties of AO-artificial zeolite. Additionally, the effects of water chemistry on the adsorption of U(VI) are investigated. It is expected that this research will provide a potential adsorbent for the removal of U(VI) from aqueous solutions in real applications.

✉ Fuqiu Ma
mafuqiu@hrbeu.edu.cn

1   Harbin Engineering University, College of Nuclear Science
     and Technology, Harbin 150001, China

2   The 404 Company Limited, China National Nuclear
     Comporation, Lanzhou 732850, China

3   The Research Center of Experimental Testing for Geology
     and Minerals, Harbin 150036, China

Materials and methods

Materials

All the chemicals are analytical grade and used without any further purification. U(VI) stock solution is made from $UO_2(NO_3)_2 * 6H_2O$ (A.R. grade). Arsenazo-III (Aladdin, China) solution is prepared by dissolving 1 g Arsenazo-III in 1000 mL of deionized water. Artificial zeolite particle is purchased from Tianjin Fuchen Chemicals, China. Polyacrylonitrile power is purchased from Daqing Petrochemical Acrylic Plant, China. Dimethyl sulfoxide (DMSO) and polyvinylpyrrolidone (PVP) are purchased from Shanghai Houcheng Chemicals.

Adsorbent preparation

4.0 g of polyacrylonitrile power is dissolved by 200 ml of dimethyl sulfoxide (DMSO). After stirring for 1 d, 8.0 g of hydroxylamine hydrochloride is added. The mixture is stirred for 5 d at 25 °C. 2 g of polyvinylpyrrolidone (PVP) and artificial zeolite are dispersed into the mixture. Then the homogeneous solution is stirred for 1 d. The AO-artificial zeolite product is washed with ethyl alcohol and deionized water 3 times and dried under vacuum at 45 °C for 24 h [22].

Batch experiment

The batch experiments are conducted in a series of 50 mL polyethylene centrifuge tubes. AO-artificial zeolite, $NaNO_3$ solution, uranium stock solution and deionized water are added to the centrifuge tubes. HNO_3 or NaOH solution is employed to adjust pH. The centrifuge tubes are shaken in a constant temperature oscillator for 3 days, after that the centrifuge tubes are centrifuged at 10000 r/min for 30 min. Supernatant is taken out to confirm the adsorption capacity of uranium using the Arsenazo-III spectrophotometric method at 652 nm. The adsorption efficiency and capacity of U(VI) on AO-artificial zeolite is calculated as follows:

$$\eta = \frac{(C_0 - C_e)}{C_0} \times 100\% \tag{1}$$

$$q_e = \frac{(C_0 - C_e)}{m} \times V \tag{2}$$

where C_0 and C_e are the initial and final concentration of U(VI), respectively; m is the mass of the adsorbent.

All of the experimental data were the averages of duplicate or triplicate experiments, and the relative errors of the data were less than 5%.

Characterization

TGA of the samples are recorded on a TA Q50 DTA/TGA apparatus in the range of 25 to 700 °C (USA). XRD measurements are obtained on a Philips X'Pert Pro Panalytical diffractometer equipped with Cu Kα radiation (scan rate 0.02°/s, $10° \leq 2\theta \leq 90°$). FT-IR are obtained using a Thermo Nicolet 6700 FT-IR spectrometer (USA) using the KBr pressed disk method. SEM is obtained using an S-4800 (Hitachi) microscope.

Results and discussion

Adsorption behavior studies

Effect of pH

The species of U(VI) and the surface charge of adsorbent in aqueous solutions can be affected by pH, thus the effect of pH is significant for U(VI) adsorption [23]. As shown in Fig. 1, it is clear that the amount of U(VI) adsorbed on artificial zeolite and AO-artificial zeolite increased with pH gradually changes from 2.5 to 6.0, whereas the adsorption percentage of U(VI) onto artificial zeolite and AO-artificial zeolite decrease with pH further increasing. Furthermore, the adsorption percentage of U(VI) onto AO-artificial zeolite

Fig. 1 Effect of pH on the U(VI) adsorption onto AO-artificial zeolite **a**; relative species distribution of U(VI) in the presence of CO_2 **b**. $m/V = 3.6$ g/L, $I = 0.01$ M $NaNO_3$, $T = 298$ K, [U(VI)] = 20 mg/L, $P_{CO_2} = 3.8 \times 10^{-4}$ atm
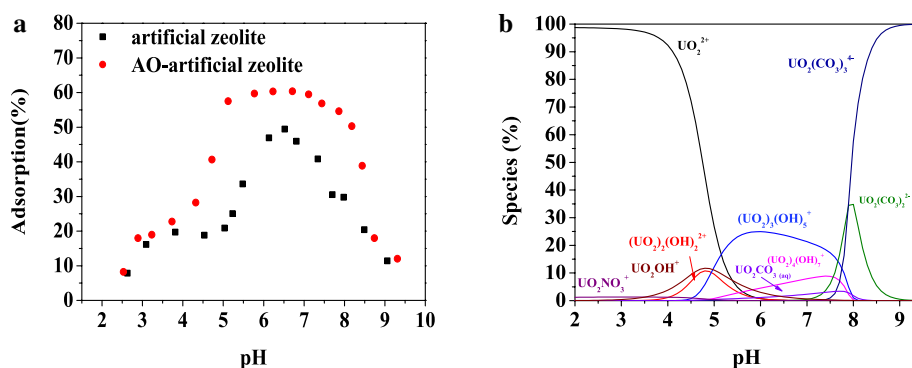
is remarkably higher than that onto artificial zeolite. There are many unbonded N and O protons in AO-groups, and these atoms may be combine with U(VI) to form chelates, the experimental result suggesting that the formation of the chelate increased the adsorption of U(VI) [24]. At lower pH, the protonation of AO-artificial zeolite and the competition between H$^+$ and U(VI) limited the adsorption of U(VI). With the pH increase, the protonation and the competition become weakened, it is easy to adsorb U(VI). Fig. 1b describes the species distribution of U(VI) depend on the pH values. At pH < 5.0, UO_2^{2+} was the main existing species of U(VI). 5.0 < pH < 7.0, the dominant species was $(UO_2)_3(OH)_5^+$. A further increase in pH value will generate negatively charged species, including $UO_2(CO_3)_2^{2-}$ and $UO_2(CO_3)_3^{4-}$, the adsorbent is not easy to adsorb negatively charged ions, the adsorption capacity declines [25].

Effect of Contact time and adsorption kinetics

Equilibration time is one of the parameters that could reflect the adsorption efficiency. The result of the effect of contact time on the adsorption of U(VI) by AO-artificial zeolite is shown in Fig. 2. The adsorption percentage of U(VI) shows an upward tendency with the contact time goes on, and reaches the maximum value within 72 h. Three different kinetic models are employed to evaluate the rate controlling process. The descriptions of pseudo-first-order, pseudo-second-order and Weber–Morris model are shown in Eqs. (3), (4) and (5), respectively:

$$q_t = q_e(1 - e^{-K_1 t}) \tag{3}$$

$$q_t = \frac{q_e^2 k_2 t}{1 + q_e k_2 t} \tag{4}$$

$$q_t = K t^{1/2} + C \tag{5}$$

where q_e and q_t are the adsorption capacity at equilibrium time and time t, respectively. k_1 and k_2 are the equilibrium rate constant of pseudo-first-order adsorption and pseudo-second-order, respectively. K (mg $*$ g^{-1} $*$ min$^{1/2}$) and C are the rate constant and adsorption constants of the Weber–Morris modal. The fitted results are summarized in Tables 1 and 2. By comparing the correlation coefficient, the adsorption of U(VI) onto AO-artificial zeolite can be fitted by pseudo-second-order kinetic model. This result is consistent with many other adsorbents [26, 27], the chemical complexing reaction dominates the adsorption process of U(VI) [28].

The Weber–Morris model explains that the adsorption process includes three steps (Fig. 2d). The first steep slope

Table 1 Kinetic parameters of pseudo-first-order and pseudo-second-order models

Pseudo-first-order model		Pseudo-second-order model	
k_1 (g/mg·min)	35.4407	k_2 (g/mg· min)	0.0175
q_e (mg/g)	3.2751	q_e (mg/g)	6.9623
R^2	0.6889	R^2	0.9830

Fig. 2 **a** Effect of contact time on the adsorption of U(VI) onto AO-artificial zeolite; **b** the fitting plot of the pseudo-first-order equation; **c** the fitting plot of the pseudo-second-order equation; **d** Weber–Morris model. pH = 5.00, m/V = 3.6 g/L, I = 0.01 M NaNO$_3$, T = 298 K, [U(VI)] = 20 mg/L
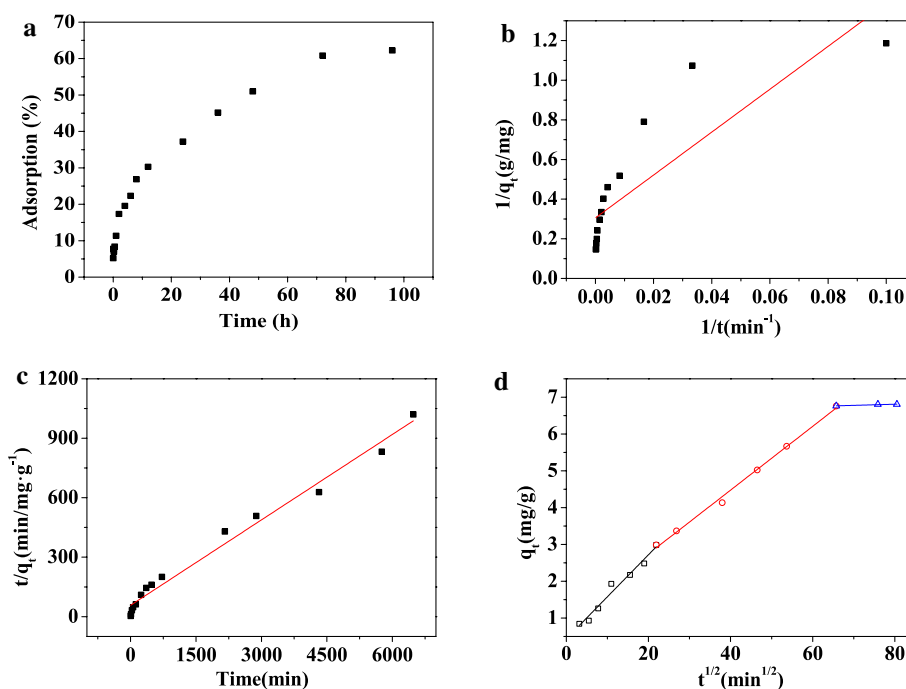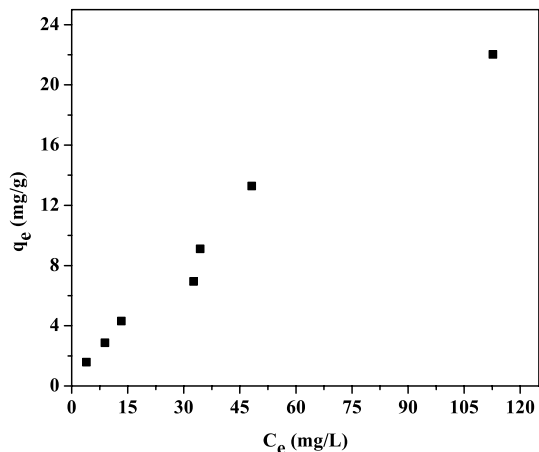
Table 2 Kinetic parameters of the Weber–Morris model

First stage		Second stage		Third stage	
k_{ad1}(g/mg· min)	0.1141	k_{ad2}(g/mg· min)	0.0866	k_{ad3}(g/mg· min)	0.0031
C_1 (μg/g)	0.4371	C_2 (μg/g)	1.0107	C_3 (μg/g)	6.5601
R_1^2	0.9704	R_2^2	0.9955	R_3^2	0.8145

Fig. 3 Effect of initial concentration of U(VI) on the adsorption on AO-artificial zeolite. pH = 5.00, m/V = 3.6 g/L, I = 0.01 M NaNO$_3$, T = 298 K

represents the external transfer step. The next stage is the intra-particle diffusion process, and the final step means the final equilibrium step [29]. The results suggest that the second stage is the rate limiting step in the process of U(VI) adsorption onto AO-artificial zeolite.

Effect of initial U(VI) concentration

The initial concentration of U(VI) provides driving forces to proceed the adsorption process [30]. Figure 3 shows the influence of the initial U(VI) concentration on the adsorption of AO-artificial zeolite for U(VI). To better understand the adsorption processes of AO-artificial zeolite to U(VI), The adsorption data were fitted by three isotherms. The Langmuir isotherm supposes that adsorption is a monolayer adsorption, and can be expressed [31]:

$$\frac{C_e}{q_e} = \frac{C_e}{q_m} + \frac{1}{K_L q_m} \tag{6}$$

The Freundlich isotherm is given as [32]:

$$lnq_e = lnK_F + \frac{1}{m}lnC_e \tag{7}$$

where K_F and n are the Freundlich constant. The Freundlich isotherm model assumes that the adsorption site is heterogeneous. The Dubinin–Radushkevich (D–R) isotherm assumes that the adsorption energy of adsorbent is nonuniform [33]. The model can be expressed [34]:

$$lnq_e = lnq_k - B\eta^2 \tag{8}$$

$$\eta = RTln\left(1 + \frac{1}{c_e}\right) \tag{9}$$

$$E = \frac{1}{\sqrt{2B}} \tag{10}$$

where B (mol^2/kJ^2) is the D–R constant, q_k (mol/g) is the D–R adsorption capacity, ε is the Polanyi potential, T is the temperature (K), and E (kJ/mol) is the free energy change [35].

The calculated linear analysis results are summarized in Table 3. The adsorption of U(VI) onto the AO-artificial zeolite obeys the Freundlich isotherm model. Therefore, the adsorption process of AO-artificial zeolite for U(VI) was considered heterogeneous and a multilayer process.

From the fitting results, the free energy change of D–R isotherm model was about 8.5 kJ/mol, indicating that the adsorption of U(VI) onto AO-artificial zeolite is mainly

Table 3 Adsorption isotherm parameters of U(VI) adsorption onto AO-artificial zeolite

Model	Freundlich model		Langmuir model		D–R model	
Parameter	n	1.2561	q_{max} (mg/g)	47.7783	B (mol^2/KJ^2)	0.0069
	K_F (L/g)	0.5246	K_L (L/mg)	7.1364×10^{-3}	q_k (mg/g)	1.0467×10^{-3}
	R^2	0.9844	R^2	0.6325	E (kJ/mol)	8.5126
					R^2	0.5475

chemical adsorption, the result is in agreement with other experimental results [36, 37].

Effect of adsorbent dosage

Adsorbent dosage determines the effective number of binding sites, so it is an important parameter in the adsorption process. The effect of adsorbent dose on U(VI) adsorption was investigated using dose range from 0.02 to 5 g/L of AO-artificial zeolite.

The data was represented in Fig. 4, the adsorption capacity of U(VI) increased from 6 to 70% at adsorbent dose from 0.02 to 5 g/L. This may be due to the increase of the available adsorption sites numbers on increasing AO-artificial zeolite dosage. However, as adsorbent dosage increases the adsorption capacity decreased. There are fewer adsorption sites on the surface of AO-artificial zeolite at lower concentration. The aggregation of particles takes place with the increase of adsorbent dosage, as a result the adsorption capacity q_e decreases. This phenomenon is also present in other adsorption systems of different adsorbents [38–40].

Characterization analysis

XRD analysis

XRD patterns of artificial zeolite and AO-artificial zeolite are shown in Fig. 5. As evident, the XRD patterns of AO-artificial zeolite do not show obvious fresh peaks
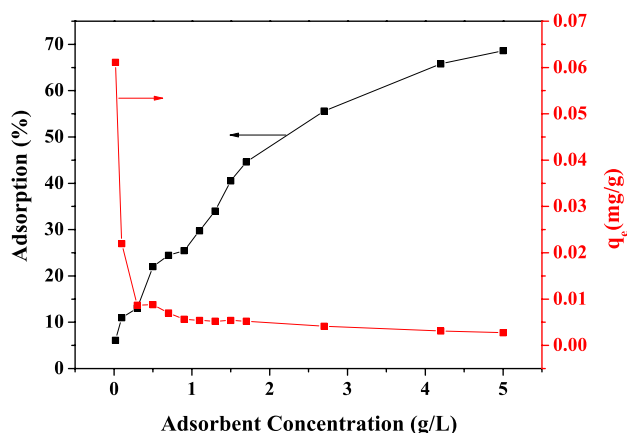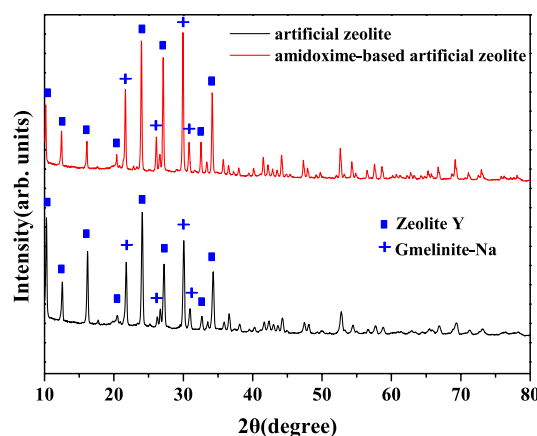
Fig. 5 XRD diffraction patterns of artificial zeolite and AO-artificial zeolite

compared with artificial zeolite, indicate that the AO-artificial zeolite maintain the original structures of artificial zeolite.

N$_2$ adsorption–desorption isotherm

The N$_2$ adsorption–desorption isotherms of artificial zeolite and AO-artificial zeolite are shown in Fig. 6. The Brunauer–Emmett–Teller (BET) surface area of artificial zeolite and AO-artificial zeolite are calculated to be 31.91 and 24.37 m^2/g, respectively. And the pore diameters are calculated to be 11.74 and 9.77 nm, respectively. This suggests that the pores of AO-artificial zeolite are partially blocked than that of artificial zeolite in the process of modification. Whereas the functional groups in AO-artificial zeolite are in favour of binding U(VI) to form chelates, which causes the AO-artificial zeolite shows better adsorption properties than artificial zeolite.

Thermogravimetric analysis

Thermogravimetric analysis is used to study the thermal behaviors of artificial zeolite and AO-artificial zeolite. As can be seen from Fig. 7, the first weight loss stage from 25 to 200 °C attributes to the elimination of physically adsorbed moisture on the surface of the particles [41]. The second weight loss occurs from 200 to 550 °C, which can be assigned to thermal decomposition of organic components. As for U(VI)-loaded AO-artificial zeolite, the weight loss observed in the range from about 250 to 600 °C may be assigned to the thermal decomposition of U(VI). Meanwhile, the weight residuals of artificial zeolite after thermal analysis is similar to that of AO-artificial

Fig. 4 Effect of adsorbent dosage on the adsorption of U(VI) onto AO-artificial zeolite. pH = 5.00, I = 0.01 M NaNO$_3$, T = 298 K, [U(VI)] = 20 mg/L

Fig. 6 Nitrogen adsorption–desorption isotherm of artificial zeolite (**a**) and AO-artificial zeolite (**b**)
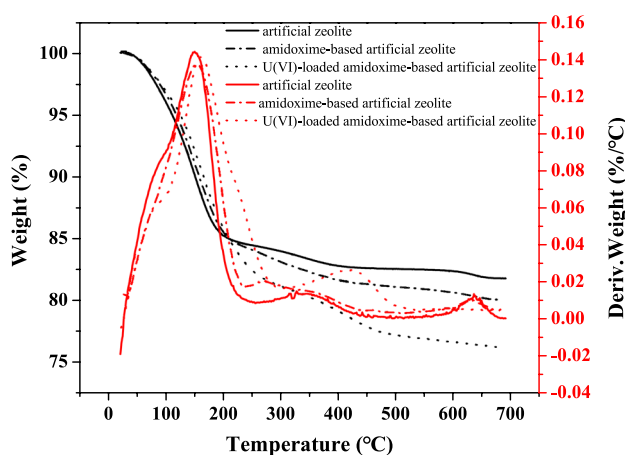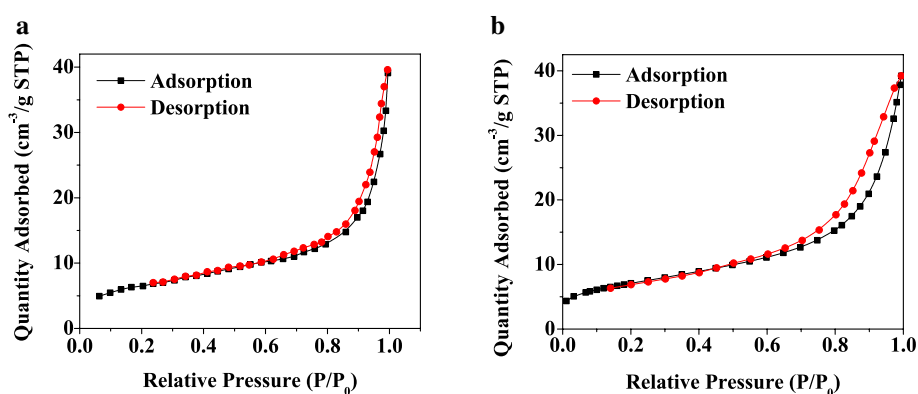
Fig. 7 Thermogravimetric analysis of artificial zeolite and AO-artificial zeolite

Fig. 8 FT-IR spectra of artificial zeolite, AO-artificial zeolite and U(VI)-loaded artificial zeolite

zeolite, the thermal stability is basically unchanged during the incorporation of AO functional groups process [42].

FT-IR analysis

FT-IR analysis is further conducted to verify the conversion of functional group in the reaction process. As shown in Fig. 8, three characteristic peaks suggest that the functional groups are grafted onto artificial zeolite successfully. The peaks at 1657 cm^{-1} could be ascribed to the stretching vibration of the $C = N$, the peaks at 1386 cm^{-1} could be ascribed to the stretching vibration of NH_2, the peaks at 945 cm^{-1} could be assigned to the bending vibration of N–O. This suggests that the amidoxime group ($HON = C - NH_2$) is covered the surface of AO-artificial zeolite. In the U(VI)-loaded AO-artificial zeolite, the peak at 750 cm^{-1} confirms the binding of uranium to AO-modified zeolite. The changes in peak positions and intensity around 550–1000 cm^{-1} region can be assigned to asymmetric stretching vibration of uranyl ion and stretching vibrations of weakly bonded oxygen ligands with uranium [43, 44].
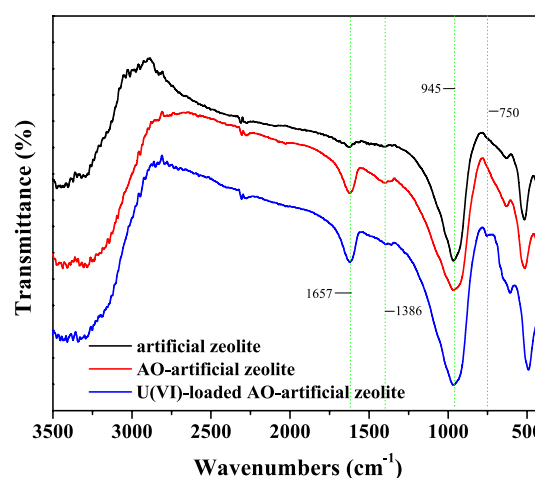
SEM analysis

The surface morphologies changes before and after artificial zeolite modified by AO are analyzed via SEM. As shown in Fig. 9a–d, after modification, the surface of AO-artificial is much rougher than artificial zeolite. Fig. 9e and f are the SEM image of AO-artificial zeolite after U(VI) adsorption. The surface of AO-artificial zeolite become rougher, a remarkable amount of particles are disposed on AO-artificial zeolite surface, which demonstrated that U(VI) is adsorbed onto the surface of AO-artificial zeolite.

Comparison with other adsorbents

The adsorption capacities of the composites for uranium were compared with other adsorbent materials reported from literature in Table 4. The comparison showed that the adsorption capacity of AO-artificial zeolite is not the best,

Fig. 9 SEM images of **a** and **b** artificial zeolite; **c** and **d** AO-artificial zeolite; **e** and **f** U(VI)-loaded AO-artificial zeolite
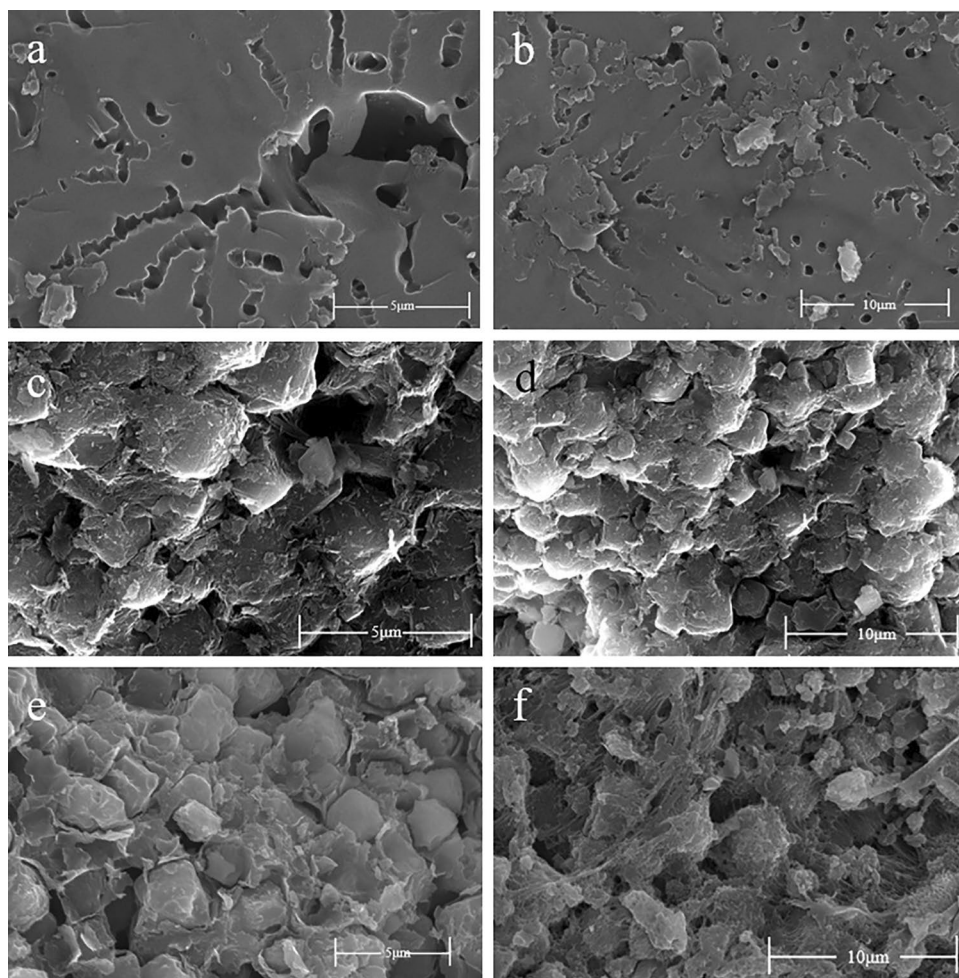

Table 4 Comparison with different adsorbents from literature

Adsorbent	Adsorption capacity (mg/g)	References
Methacryloxypropyltrimethoxysilane coated magnetic	1.1	[45]
Modified magnetic Fe_3O_4	12.33	[46]
Used tires	10.1	[47]
Natural clinoptilolite zeolite	2.12	[48]
CuO/NaX nanocomposite	6.77	[49]
β-cyclodextrin functionalized silica gel	6.45	[50]
Magnetite nanoparticles	4.76	[51]
Tendurek volcanic tuff	2.38	[52]
MnO coated sand	4.76	[53]
Amidoximated polyglycidyl methacrylate microbeads	1.07	[54]
AO-artificial zeolite	6.96	This work

nonetheless it is a relatively inexpensive material in all of them. It owns high cost performance, and can be used as an alternative material for commercial applications.

Conclusions

In this study, the adsorption of U(VI) onto AO-artificial zeolite is investigated. The consequence of adsorption indicated that AO-artificial zeolite had high removal

amount towards U(VI), which is much higher than that of artificial zeolite, adsorption capacity of U(VI) is significantly enhanced. Furthermore, AO-artificial zeolite overcome the defect of disperse in aqueous during adsorption process, which could offer a promising opportunities for further improvements in the removal of U(VI) from aqueous solution.

Compliance with ethical standards

Conflict of interest The authors declare that they have no conflict of interest.

References

1. Lv Z, Wang H, Chen C, Yang S, Chen L, Alsaedi A, Hayat T (2019) Enhanced removal of uranium(VI) from aqueous solution by a novel Mg–MOF-74-derived porous MgO/carbon adsorbent. J Colloid Interface Sci 537:1–10

2. Su S, Liu Q, Liu J, Zhang H, Li R, Jing X, Wang J (2018) Polyethyleneimine-functionalized Luffa cylindrica for efficient uranium extraction. J Colloid Interface Sci 530:538–546

3. Duan S, Xu X, Liu X, Wang Y, Hayat T, Alsaedi A, Meng Y, Li J (2018) Highly enhanced adsorption performance of U(VI) by non-thermal plasma modified magnetic Fe_3O_4 nanoparticles. J Colloid Interface Sci 513:92–103

4. Duan S, Liu X, Wang Y, Shao D, Alharbi NS, Alsaedi A, Li J (2016) Highly efficient entrapment of U(VI) by using porous magnetic $Ni_{0.6}Fe_{2.4}O_4$ micro-particles as the adsorbent. J Taiwan Inst Chem Eng 65:367–377

5. Lapka JL, Paulenova A, Alyapyshev MY, Babain VA, Herbst RS, Law JD (2009) Extraction of uranium(VI) with diamides of dipicolinic acid from nitric acid solutions. Radiochimica Acta 97(6):291–296

6. Tsaoulidis D, Ortega EG, Angeli P (2018) Intensified extraction of uranium(VI) in impinging-jets contactors. Chem Eng J 342:251–259

7. Pidchenko I, Kvashnina KO, Yokosawa T, Finck N, Bahl S, Schild D, Polly R, Bohnert E, Rossberg A, Gottlicher J et al (2017) Uranium redox transformations after U(VI) coprecipitation with magnetite nanoparticles. Environ Sci Technol 51(4):2217–2225

8. Rezaee M, Khalilian F (2015) Determination of uranium in water samples using homogeneous liquid–liquid microextraction via flotation assistance and inductively coupled plasma-optical emission spectrometry. J Radioanal Nuclear Chem 304(3):1193–1200

9. Gao MW, Zhu GR, Wang XH, Wang P, Gao CJ (2015) Preparation of short channels SBA-15-PVC membrane and its adsorption properties for removal of uranium(VI). J Radioanal Nuclear Chem 304(2):675–682

10. Li P, Wang J, Wang Y, Liang J, He B, Pan D, Fan Q, Wang X (2019) Photoconversion of U(VI) by TiO_2: an efficient strategy for seawater uranium extraction. Chem Eng J 365:231–241

11. Wang X, Ding C, Xiangxue C, Wencai S, Yubing Z (2016) Adsorption of U(VI) on sericite in the presence of bacillus subtilis: a combined batch, EXAFS and modeling techniques. Geochimica et Cosmochimica Acta: J Geochem Soc Meteorit Soc 180:51–65

12. Hu T, Ding S, Deng H (2016) Application of three surface complexation models on U(VI) adsorption onto graphene oxide. Chem Eng J 289:270–276

13. Zhu K, Lu S, Gao Y, Zhang R, Tan X, Chen C (2017) Fabrication of hierarchical core–shell polydopamine@MgAl − LDH_s composites for the efficient enrichment of radionuclides. Appl Surf Sci 396:1726–1735

14. Yu X, Helvenston EM, Shuller-Nickles LC, Powell BA (2016) Surface complexation modeling of Eu(III) and U(VI) interactions with graphene oxide. Environ Sci Technol 50:1821–1827

15. Chen H, Chen Z, Zhao G, Zhang Z (2018) Enhanced adsorption of U(VI) and ^{241}AM(III) from wastewater using Ca / Al layered double hydroxide@carbon nanotube composites. J Hazard Mater 347:67–77

16. Yue Y, Mayes RT, Kim J, Fulvio PF, Sun XG, Tsouris C, Chen J, Brown S, Dai S (2013) Seawater uranium sorbents: preparation from a mesoporous copolymer initiator by atom-transfer radical polymerization. Angewandte Chemie Int Ed 52(50):13458–13462

17. Yuan D, Long C, Xin X, Yuan L, Liao S, Wang Y (2015) Removal of uranium(VI) from aqueous solution by amidoxime functionalized superparamagnetic polymer microspheres prepared by a controlled radical polymerization in the presence of DPE. Chem Eng J 285:358–367

18. Tan L, Liu Q, Jing X, Liu J, Song J, Hu S, Liu L, Wang J (2015) Removal of uranium(VI) ions from aqueous solution by magnetic cobalt ferrite/multiwalled carbon nanotubes composites. Chem Eng J 273:307–315

19. Yang W, Bai ZQ, Shi WQ, Yuan LY, Tian T (2013) MOF-76: from a luminescent probe to highly efficient U(VI) sorption material. Chem Commun 49:10415–10417

20. Zhao Y, Wang X, Li J, Wang X (2015) Amidoxime functionalization of mesoporous silica and its high removal of U(VI). Polym Chem 6:5376–5384

21. Xiao J, Jing Y, Yao Y, Wang X, Jia Y (2019) Synthesis of amidoxime-decorated 3D cubic mesoporous silica via self-assembly co-condensation as a superior uranium(VI) adsorbent. J Mol Liq 277:843–855

22. Ladshaw AP, Wiechert AI, Sadananda D, Sotira Y, Costas T (2017) Amidoxime polymers for uranium adsorption: influence of comonomers and temperature. Materials 10:1268

23. Wang Y, Wang Z, Ang R, Yang J, Liu N, Liao J, Yang Y, Tang J (2015) Synthesis of amidoximated graphene oxide nanoribbons from unzipping of multiwalled carbon nanotubes for selective separation of uranium(VI). RSC Adv 5:89309–89318

24. Zhang Z, Dong Z, Wang X, Ying D, Niu F, Cao X, Wang Y, Hua R, Liu Y, Wang X (2018) Ordered mesoporous polymer–carbon composites containing amidoxime groups for uranium removal from aqueous solutions. Chem Eng J 341:208–217

25. Xingjun W, Guojia J, Guiru Z, Chenghao S, Han Z, Congjie G (2019) Surface hydroxylation of SBA-15 via alkaline for efficient amidoxime-functionalization and enhanced uranium adsorption. Sep Purif Technol 209:623–635

26. Peng W, Huang G, Yang S, Guo C, Shi J (2019) Performance of biopolymer/graphene oxide gels for the effective adsorption of U(VI) from aqueous solution. J Radioanal Nuclear Chem 322(2):861–868

27. Wang Z, Zhao D, Wu C, Chen S, Wang Y, Chen C (2020) Magnetic metal organic frameworks/graphene oxide adsorbent for

the removal of U(VI) from aqueous solution. Appl Radiat Isot 162:109160

28. Li W, Liu Q, Liu J, Zhang H, Li R, Li Z, Jing X, Wang J (2017) Removal U(VI) from artificial seawater using facilely and covalently grafted polyacrylonitrile fibers with lysine. Appl Surf Sci 403:378–388

29. Hai NT, You SJ, Hosseini-Bandegharaei A, Chao HP (2017) Mistakes and inconsistencies regarding adsorption of contaminants from aqueous solutions: a critical review. Water Res 120:88–116

30. We X, Liu Q, Zhang H, Liu J, Wang J (2017) Rapid and efficient uranium(VI) capture by phytic acid/polyaniline/ FeOOH composites. J Colloid Interface Sci 511:1–11

31. Guibal E, Milot C, Tobin JM (1998) Metal-anion sorption by chitosan beads: equilibrium and kinetic studies. Indus Eng Chem Res 37(4):1454–1463

32. Freundlich H (1907) Über die adsorption in lösungen. Zeitschrift für Physikalische Chemie 57(1):385–470

33. Yang P, Liu Q, Liu J, Chen R, Li R, Bai X, Wang J (2018) Highly efficient immobilization of uranium(VI) from aqueous solution by phosphonate-functionalized dendritic fibrous nanosilica (DNFS). J Hazard Mater 363:248–257

34. Dabrowski A (2001) Adsorption-from theory to practice. Adv Colloid Interface Sci 93:135–224

35. Duan S, Xu X, Liu X, Wang Y, Li J (2017) Highly enhanced adsorption performance of U(VI) by non-thermal plasma modified magnetic Fe_3O_4 nanoparticles. J Colloid Interface Sci 513:92–103

36. Imam EA, Elsayed I, Mahfouz MG, Tolba AA, Akashi T, Galhoum AA, Guibal E (2018) Synthesis of α-aminophosphonate functionalized chitosan sorbents: effect of methyl versus phenyl group on uranium sorption. Chem Eng J 352:1022–1034

37. Zhang Z, Duan S, Chen H, Fengsong Z, Hayat T, Ahmed A, Jiaxing L (2018) Synthesis of porous magnetic $Ni_{0.6}Fe_{2.4}O_4$ nanorods for highly efficient adsorption of U(VI). J Chem Eng Data ACS J Data 63(5): 1810–1820

38. Wang XK, Chen CL, Zhou X, Tan XL, Hu WP (2005) Diffusion and sorption of U(VI) incompacted bentonite studied by a capillary method. Radiochim Acta 93:273–278

39. Lu Z, Yalou S, Lijuan S, Xiangchen S, Suwen C, Wangsuo W (2016) Dihydroxy bezladely derivatives functionalized mesoporous silica SBA-15 for the sorption of U(VI). J Radioanal Nuclear Chem 310:125–137

40. Padmavathy KS, Madhu G, Haseena PV (2016) A study on effects of pH, adsorbent dosage, time, initial concentration and adsorption isotherm study for the removal of hexavalent chromium (Cr(VI)) from wastewater by magnetite nanoparticles. Proc Technol 24:585–594

41. Sun Y, Shao D, Chen C, Yang S, Wang X (2013) Highly efficient enrichment of radionuclides on graphene oxide-supported polyaniline. Environ Sci Technol 47(17):9904–9910

42. Nakkeeran E, Selvaraju N (2017) Biosorption of chromium(VI) in aqueous solutions by chemically modified strychnine tree fruit shell. Int J Phytoremediation 19(12):1065–1076

43. Saini AS, Melo JS (2013) Biosorption of uranium by melanin: kinetic, equilibrium and thermodynamic studies. Bioresour Technol 149:155–162

44. Cejka J (1999) Infrared spectroscopy and thermal analysis of the uranyl minerals. Rev Mineral Geochem 38:520–622

45. Tavengwa Nikita Tawanda, Cukrowska E, Chimuka L (2014) Preparation, characterization and application of $NaHCO_3$ leached bulk U(VI) imprinted polymers endowed with γ-MPS coated magnetite in contaminated water. J Hazard Mater 267:221–228

46. Sadeghi S, Azhdari H, Arabi H, Moghaddam AZ (2012) Surface modified magnetic Fe_3O_4 nanoparticles as a selective sorbent for solid phase extraction of uranyl ions from water samples. J Hazard Mater 215–216:208–216

47. Mahramanlioglu M (2003) Adsorption of uranium on adsorbents produced from used tires. J Radioanal Nuclear Chem 256(1):99–105

48. Camacho LM, Parra RR, Deng S (2011) Uranium removal from groundwater by natural clinoptilolite zeolite: effects of pH and initial feed concentration. J Hazard Mater 189(1–2):286–293

49. Abdi MR, Shakur HR, Saraee KRE, Sadeghi M (2014) Effective removal of uranium ions from drinking water using CuO/X zeolite based nanocomposites: effects of nano concentration and cation exchange. J Radioanal Nuclear Chem 300(3):1217–1225

50. Liu HJ, Jing PF, Liu XY, Du KJ, Sun YK (2016) Synthesis of β-cyclodextrin functionalized silica gel and its application for adsorption of uranium(VI). J Radioanal Nuclear Chem 310(1):1–8

51. Das D, Sureshkumar MK, Koley S, Mithal N, Pillai CGS (2010) Sorption of uranium on magnetite nanoparticles. J Radioanal Nuclear Chem 285:447–454

52. Yusan S, Aslani MAA, Turkozu DA, Aycan HA, Aytas S, Akyil S (2010) Adsorption and thermodynamic behaviour of U(VI) on the Tendurek volcanic tuff. J Radioanal Nuclear Chem 283:231–238

53. Zou W, Zhao L, Han R (2011) Adsorption characteristics of uranyl ions by manganese oxide coated sand in batch mode. J Radioanal Nuclear Chem 288:239–249

54. Caykara T, Alaslan SS, Inam R (2010) Competitive adsorption of uranyl ions in the presence of Pb(II) and Cd(II) ions by poly(glycidyl methacrylate) microbeads carrying amidoxime groups and polarographic determination. J Appl Polym Ence 104:4168–4172